# Detection of Obscured Targets with IR Polarimetric Imaging

J. Larry Pezzaniti, David Chenault
Polaris Sensor Technologies

Kris Gurton, Melvin Felton
US Army Research Labs, Adelphi MD

## Abstract

A polarization thermal sensor is presented that has ability to detect manmade objects even when there is little or no thermal contrast, or when the object is obscured by clutter or vegetation. Imagery will be shown for scenarios in which polarization contrast remains high during periods of zero thermal contrast. Also, data will be presented that shows the detection of manmade targets in natural clutter, long after thermal equilibrium of the target with the background has been established.

## 1. Introduction

Thermal LWIR microbolometer cameras are becoming more and more ubiquitous. The application space (and market) for these systems grow as the cost of the device continues to come down. They are used in military applications for acquiring and tracking targets from a multitude of platforms, and in the commercial industry for heat detection, security, surveillance and recently in automotive applications. A LWIR microbolometer is a very effective technology that fills the needs for many applications. Still, thermal imaging often falls short in situations involving high clutter and low thermal contrast.[1-4]

In this paper we present a small light weight LWIR imaging polarimeter that measures both the **thermal** and **polarization** content of an image. An imaging polarimeter is especially effective when thermal contrast is low or when the target becomes hidden in the background.

**Figure 1** shows an example image from a military application. The image is taken late at night after the vehicle has come to thermal equilibrium with its background.

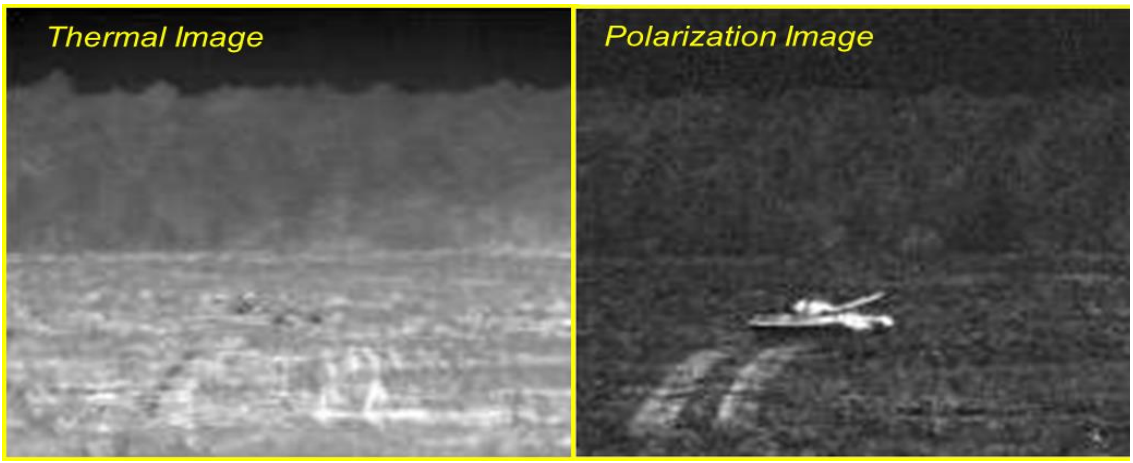


**Figure 1** Comparison of thermal and polarization image.

That is, the temperature of the tank equals the temperature of the background. The thermal image shows that the thermal contrast is essentially zero. It is further complicated by the fact that the spatial frequencies in the tank image are nearly equal to the background. The tank is essentially invisible in the thermal image.

In the polarization image, however, the tank is clearly visible. The reason for this is that the tank reflects and emits polarization states different due to its surface properties and geometry. A LWIR imaging polarimeter measures the differences in emitted and reflected polarization. The polarization image in **Figure 1** is the difference between horizontally polarized and vertically polarized light.

It is important to note that an imaging polarimeter provides both a thermal image that the user is accustomed to viewing as well as a polarization image. The user is able to switch between thermal and polarization mode. A hybrid thermal/polarization mode is also available.

This describes a new commercially available imaging polarimeter called SPYDER. Other imaging polarimeters have been developed for the LWIR portion of the spectrum. [5,6] This system is small and lightweight. The sensor head weighs 20oz and was designed for the dismounted soldier. **Figure 2** shows SPYDER mounted to the helmet of a soldier.

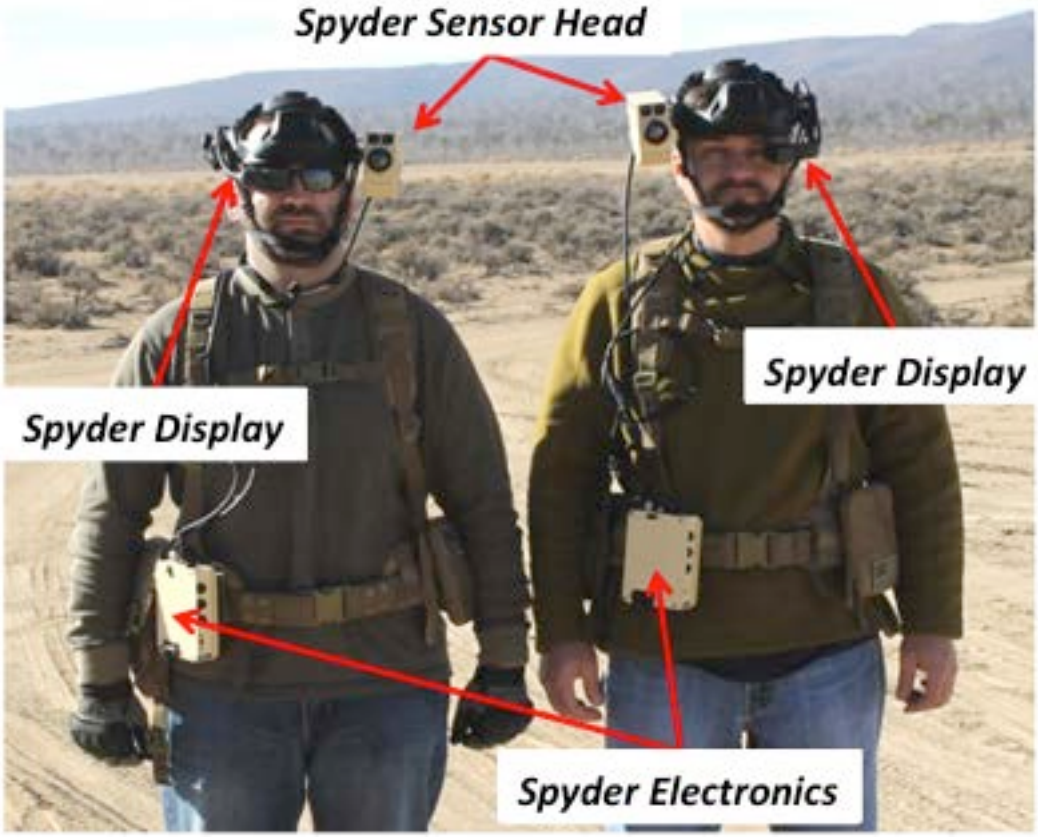


**Figure 2** SPYDER LWIR imaging polarimeter on dis-mounted personnel.

The sensor head is adaptable to various user preferences. It can be used easily with or without tactical gloves and/or sunglasses. The sensor head can either be mounted on the right or the left side of the helmet or Ops-Core Skull Crusher, and operates from either a standard 2590 battery or AA-batteries (AN-PRC-152, -148 battery compatibility is also possible). The user also has a choice of helmet mounted displays; either a Tac-Eye, a Liteye, or any customer display that accepts NTSC video input. Because it is hands-free, the SPYDER system can easily be combined with other detection methodologies to optimize total performance.

Because the sensor is small, rugged and lightweight, it can be mounted to a variety of user platforms such as UAS, Ground Vehicles or stationary platforms.

The remainder of this paper will describe the SPYDER LWIR imaging polarimeter, provide the basis for its measurement and show some example data that illustrates the utility of the sensor.

## 2. SPYDER LWIR imaging polarimeter

The SPYDER LWIR imaging polarimeter represents the smallest most compact and integrated imaging polarimeter available. It was originally developed for as a hands-free helmet mounted sensor for the dismounted soldier to assist in locating potential IED emplacements for route clearance, identifying safe passage routes to avoid all possible emplacement locations, detecting areas of traffic including footprints, footpaths and trails, and tire tracks. **Figure 3** shows the components of the SPYDER sensor. It consists of the sensor head, user interface electronics which is tethered to the sensor head and a heads up display.

The sensor head mounted to the helmet weighs 20 oz. and is adaptable to various user preferences. It can be used easily with or without tactical gloves and/or sunglasses.

**Table 1** Specifications for SPYDER

| Parameter | Value |
|---|---|
| Pixel Format | 320 x 256 |
| Horizontal FOV | 30° |
| Frame Rate | 30 fps |
| Video out | NTSC |
| Output modes | Thermal, $s_1$ polarization |
| User interface | Vest mounted buttons |
| Sensor head weight | 20 oz. |
| Power | 8 |
| Run time | 1 ½ hours (continuous) |

The sensor head can either be mounted on the right or the left side of the helmet or Ops-Core Skull Crusher, and operates from either a standard 2590 battery or AA-batteries (AN-PRC-152, -148 battery compatibility is also possible). The user also has a choice of helmet mounted displays; either a Tac-Eye, a Liteye, or any customer display that accepts NTSC video input. Because it is hands-free, the SPYDER system can easily be combined with other detection methodologies to optimize total performance.

Preliminary test and evaluation shows that utilizing the SPYDER system to locate potential IED emplacements requires minimal training; less than an hour to master the user interface (including adjustments for user preferences) and approximately 8 hours to become proficient in recognizing the signature of emplacements.

**Table 1** shows the specifications for SPYDER. SPYDER measures two images of orthogonal polarization simultaneously. One state of polarization is parallel to the short axis of the sensor (horizontal linear polarization) and the second state is parallel to the long axis of the sensor (vertical linear polarization). Since the symmetry axis of polarization is most often

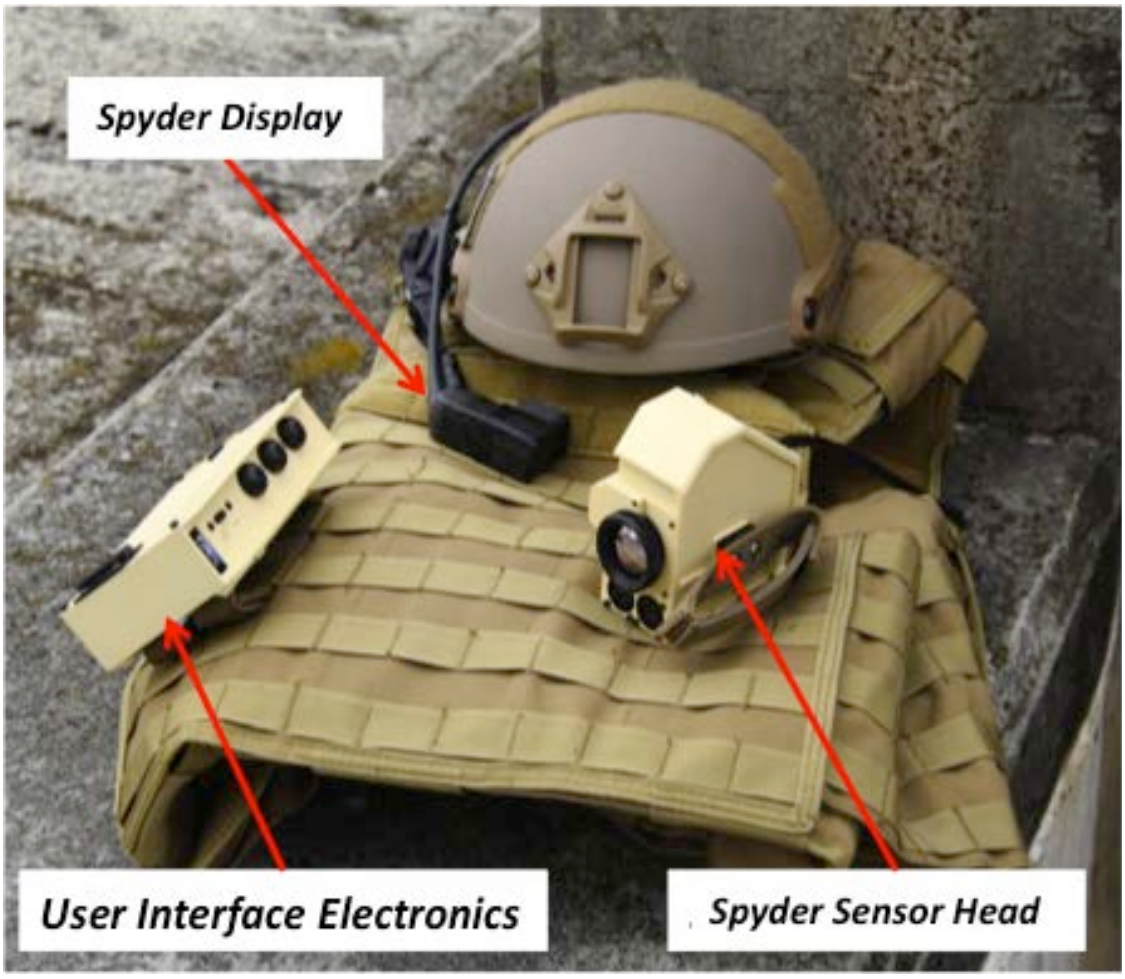


**Figure 3** SPYDER sensor components.

To operate the SPYDER, the user interface consists of four push buttons. On power up, the system pauses on a splash screen while user adjusts the helmet mounted display to optimize its performance. A single push of a button resumes normal operation in which the system automatically calibrates itself and displays the requisite imagery for location of potential IED emplacements. To add capability and adaptability to environment and changing conditions, the user can select from a suite of data output settings that allow the SPYDER to provide useful information even in challenging conditions like that found in the thermal shadow of a wall, or in other areas of high dynamic contrast. A "power user" interface allows the user to view images that are fundamental to the operation of the SPYDER.

The SPYDER is simple to use, easily configurable, light weight, and low power. Users can easily learn to utilize its features; one new user was correctly identifying emplacements with less than 2 hours of training in a controlled environment.

## 3. Emission and Reflection Polarization

Thermal polarization is described in varying detail in the following references [6,7,8,9]. To understand the polarization signature of a surface it is instructive to develop the equations for polarized light emanating from a smooth surface. To understand thermal polarization, we must start with Kirkoff's law stating that spectral emissivity, $\varepsilon$ of a surface equals spectral absorptivity, $\alpha$ of that surface and

$$\varepsilon(\lambda, T, \theta) = \alpha(\lambda, T, \theta) = 1 - r(\lambda, T, \theta), \quad (1)$$

where $r$ is that surface's reflectance, $\lambda$ is the wavelength of emission or reflected light, $T$ is the temperature of that surface and $\theta$ is the angle of emission or reflection from the surface within the plane of incidence, see **Figure 4**. Two components of linear emissive or reflected polarization are defined to be parallel to the plane of incidence (defined by the reflected or emitted ray and the surface normal) and orthogonal to the plane of incidence. The corresponding Kirkoff's equations are

$$\varepsilon_{\parallel}(\lambda, T, \theta) = 1 - r_{\parallel}(\lambda, T, \theta) \quad (2)$$

$$\varepsilon_{\perp}(\lambda, T, \theta) = 1 - r_{\perp}(\lambda, T, \theta) \quad (3)$$

where $\parallel$ indicates emissivity or reflectivity of light linearly polarized in the plane of incidence and $\perp$ indicates emissivity or reflectivity of light linearly polarized perpendicular to the plane of incidence.

The polarization state of light emanating from a surface is composed of both emitted and reflected thermal radiation. The polarization state can be expressed as a Stokes vector in terms of the radiance values emerging from the surface.

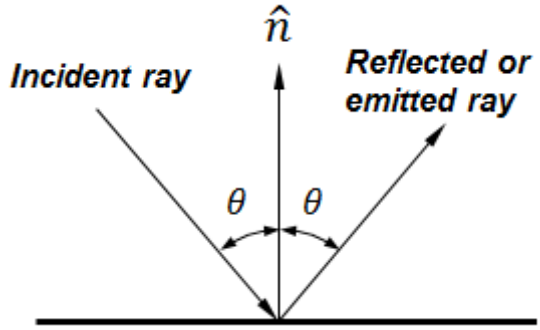


**Figure 4** Angle of incidence

The Stokes vector is defined as, $$\vec{S} = \begin{bmatrix} s_o \\ s_1 \\ s_2 \end{bmatrix} = \begin{bmatrix} L_\perp + L_\parallel \\ L_\perp - L_\parallel \\ L_{45} - L_{135} \end{bmatrix} \quad (4)$$

$L_\parallel$ is the radiance of light polarized parallel to the plane of incidence given by

$$L_\parallel(\lambda, T, \theta) = \int_{\lambda_1}^{\lambda_2} \varepsilon_\parallel(\lambda, T, \theta) \cdot L_S(\lambda, T) \cdot d\lambda + \int_{\lambda_1}^{\lambda_2} r_\parallel(\lambda, T, \theta) \cdot L_B(\lambda, T) \cdot d\lambda \quad (5)$$

where $\lambda_1$ and $\lambda_2$ define the waveband of interest, $L_S(\lambda, T)$ is the blackbody radiation of the surface at temperature $T$, and $L_B(\lambda, T)$ is the background radiance reflected from the surface along the ray path within the plane of incidence defined by angle $\theta$. Similarly,

$$L_\perp(\lambda, T, \theta) = \int_{\lambda_1}^{\lambda_2} \varepsilon_\perp(\lambda, T, \theta) \cdot L_S(\lambda, T) \cdot d\lambda + \int_{\lambda_1}^{\lambda_2} r_\perp(\lambda, T, \theta) \cdot L_B(\lambda, T) \cdot d\lambda \quad (6)$$

From equations (4), (5), and (6) we can write

$$s_1 = \int_{\lambda_1}^{\lambda_2} (r_\perp - r_\parallel) \cdot (L_B - L_S) \cdot d\lambda \quad (7)$$

where here we suppress the $\lambda, T, \theta$ dependencies to simplify the notation. Similarly we have

$$s_0 = \int_{\lambda_1}^{\lambda_2} (L_S + r \cdot (L_B - L_S)) \cdot d\lambda \quad (8)$$

The Stokes vector element $s_2$ appears when the plane of emission is rotated with respect to the detecting sensor.

To interpret these equations we can see that according to equation (7) for a smooth surface, a non-zero $s_1$ Stokes vector requires that the $L_B \neq L_s$ and $r_\perp \neq r_\parallel$. For many out-door situations, the condition $L_B \neq L_s$ is met, because surfaces tend to reflect sky background down-welling radiation that is significantly smaller than the emission of objects on the ground. For example, in the LWIR, if the sky apparent temperature is -20C, and the ground apparent temperature is 20C, then $L_B \sim \frac{1}{2} L_s$. On a cloudy summer day, the down-welling radiance can be closer to the emitted radiance of objects on the ground, but they will rarely be equal.

Secondly the parallel and perpendicular components of reflectance cannot be equal, $r_\perp \neq r_\parallel$. The difference $(r_\perp - r_\parallel)$ can be a strong function of surface roughness, the surface complex refractive index, angle of emission$\theta$, and wavelength $\lambda$. The difference $(r_\perp - r_\parallel)$ is a good source of contrast between an object of interest and its background. For example, for many man-made surfaces such as metal surfaces, glass, plastics, ceramics, this condition is met $r_\perp$ and $r_\parallel$ can differ by several percent. However, for many natural surfaces such as dirt, grass, trees, rocks, shrubs which are very rough, $r_\perp$ is nearly equal to or exactly equal to $r_\parallel$ .

Thus the contrast in an image of $s_1$, which is based on the difference of $(r_\perp - r_\parallel)$ between the target of interest and the background, is often still significant even when the apparent temperature of the target equals the apparent temperature of the background.

## 4. Thermal Contrast vs Polarization Contrast

LWIR imaging polarimetry has two primary advantages over standard thermal imaging. The first advantage, pointed out in the introduction, is the ability to detect in zero thermal contrast. A second advantage of polarimetry is background clutter rejection.

**Figures 5 and 6** compare the thermal and polarization imagery taken from a Corvus LWIR imaging polarimeter also offered by Polaris Sensor Technologies.[7] The image is taken from an altitude of 450 feet, approximately 1 km from the target. Both targets 1 and 2 are clearly visible in the IR polarized image. Target number 1 is also visible in the IR thermal image, but could easily be confused with several shrubs and other natural features surrounding Target 1. Target 2 completely blends into the roadway background and is not visible in the IR thermal image. Target 2 is only visible in the IR polarized image. Target 2 is invisible (zero contrast) in the IR thermal because it's apparent temperature equals the apparent temperature of the surrounding roadway. Zero contrast conditions often occur when the target has been at rest for several hours (no heat load from engine) or the target is camouflaged. Low contrast of 'at rest' or camouflaged targets is typically observed during two periods of the diurnal cycle. Those times depend primarily on the ambient temperature and solar loading profiles of a given day, along with parameters such as the thermal capacity and emissivity of the targets and backgrounds. Those times of day when the apparent temperatures of target and backgrounds are equal (zero contrast) are referred to as cross-over points. A significant advantage of polarimetry for target acquisition is that it still sees the target at those cross-over points.

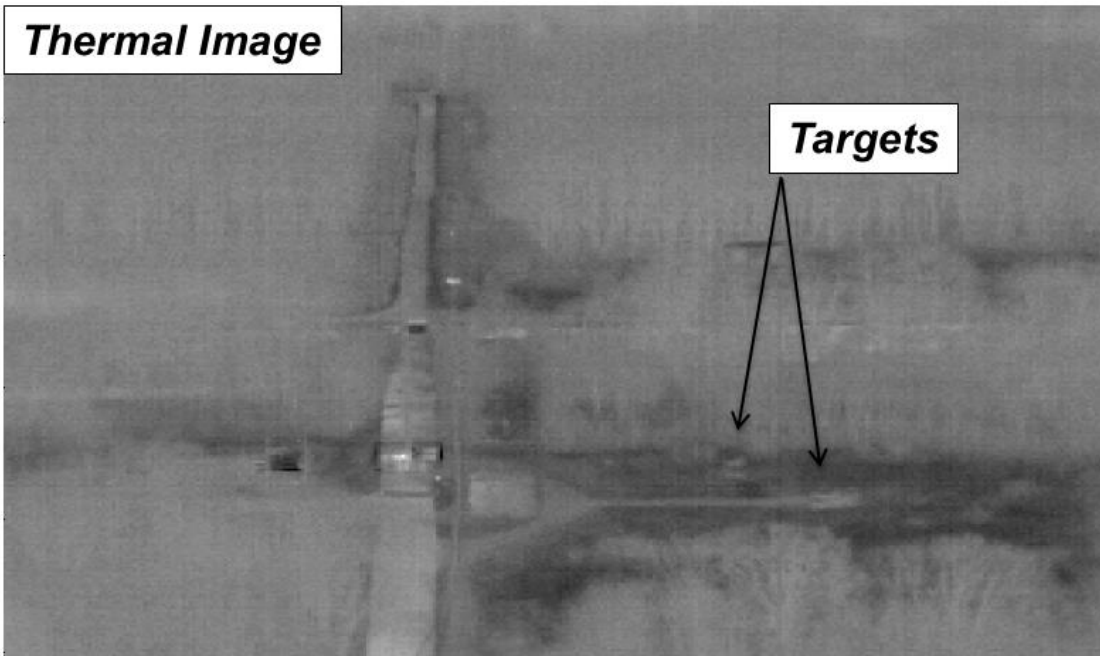


**Figure 5** Standard LWIR thermal image of scene with two military targets. Image captured with a Corvus LWIR imaging polarimeter.

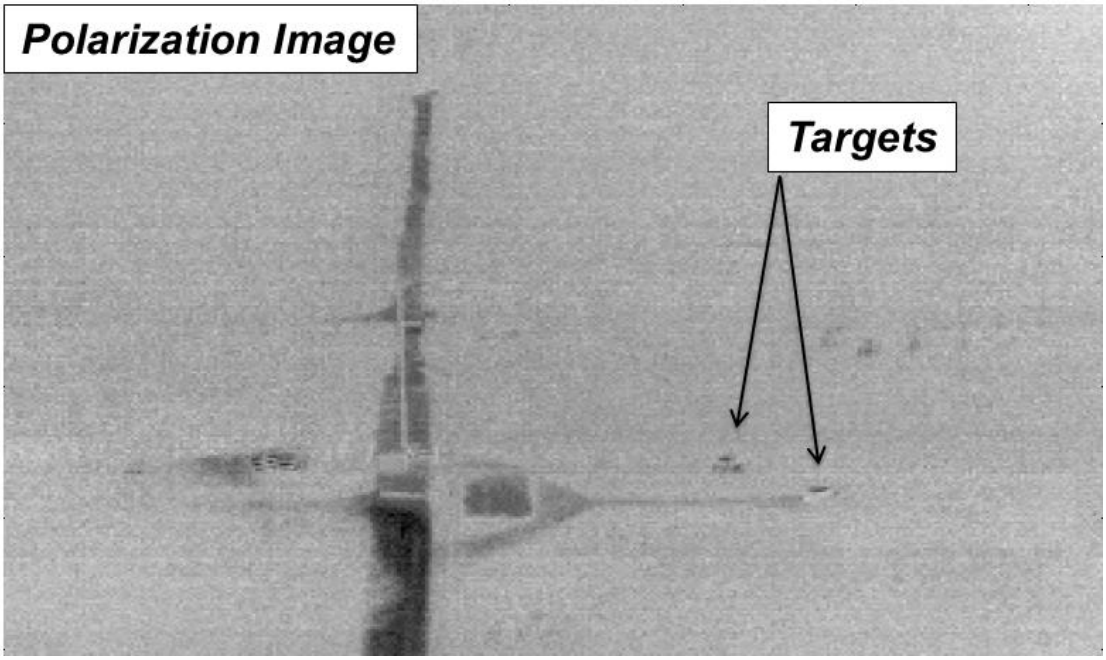


**Figure 6** Polarimetric LWIR image of same scene as in **Figure 1**. Natural background of trees, shrubs, dirt, rocks is rejected in the polarized image because it is unpolarized. Military targets are partially polarized.

Note the complexity of the IR image compared to the Polarized image. Virtually all of the natural features such as trees, shrubs, large boulders, bald spots in the grass - all of which can take on the apparent size and temperature of a target of interest - are rejected in the polarized image. This level of discrimination from the sensor itself has the potential to greatly enhance the robustness of target acquisition, tracking and discrimination algorithms used in an air to ground seeker.

The physics that governs thermal and polarization signatures depends on the temperature, material and surface roughness of the target and background, the down-welling radiance, earth albedo, aspect angle, path radiance and several other parameters. Because these parameters change with waveband (either MWIR or LWIR), the thermal and polarization signatures also change with waveband. When polarization or thermal contrast is poor in the MWIR, it is often better in the LWIR and vice versa. Thus combining the MWIR and LWIR in one sensor can increase the robustness of detection tremendously.

**Figure 7** shows data from a LWIR imaging polarimeter. Two 18" x 18" Mylar panels are placed in an open field. The temperatures of the Mylar panels are controllable by passing current through resistive wire embedded in the Mylar. The Mylar panels are labeled 1 and 2 in the thermal images. The ambient temperature of the ground during this experiment was approximately 29C. The temperature of Mylar panel 1 was set to approximately 27C. The temperature of Mylar panel 2 was adjusted from just above 28C to approximately 29.5C. A movie of the panels was recorded over the course of about 1 minute as the temperature of Mylar panel 2 changed linearly from 28C to 29.5C.

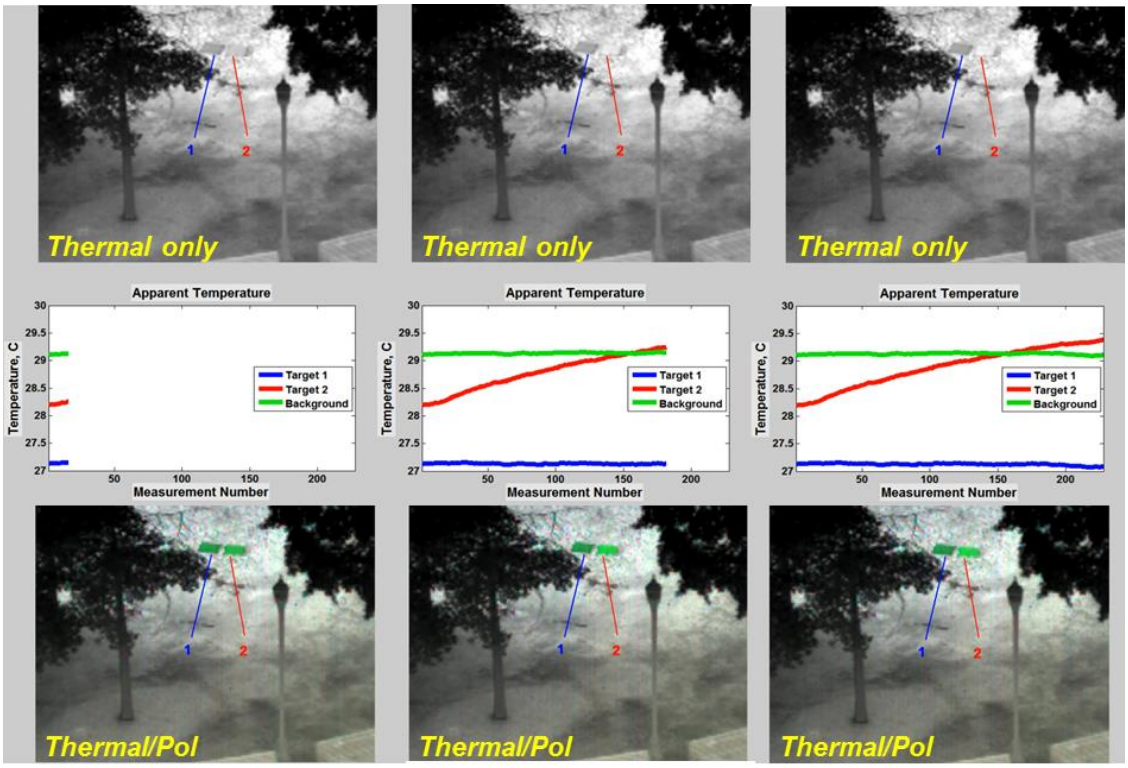


**Figure 7** Polarization of targets during thermal cross-over point.

The imaging polarimeter recorded both thermal and polarization images at a rate of 30 fps from an altitude of 50ft at a standoff distance of approximately 300ft. Figure 5 is organized as follows. The top row is the three different thermal images corresponding to when Mylar panel 2 was at three different temperatures. The middle row shows the plots of the temperatures (sampled at 4 Hz) of the two panels and the ground over the 1 minute time frame. The bottom row is the thermal image with polarization overlaid in color. The left column shows the thermal and polarization images when Mylar panel 2 was cooler than the background, the middle column shows where the temperature of Mylar panel 2 equaled the background temperature, and the right shows Mylar panel 2 at a higher temperature than the background. Note that the polarization $s_1$ contrast remains high in spite of the thermal contrast passing through zero.

**Figure 8** shows a plot of $s_1$ for Mylar panel 1 (held at 27C), Mylar panel 2 that changed temperature and the ground. Note that the polarization of the ground remained low <0.0025. The polarization of Mylar panel remained constant at approximately 0.035, and the polarization of Mylar panel 2 increased only slightly.

**Figures 9** and **10** present another experiment where the LWIR imaging polarimeter was panned across an area of ground with several Mylar targets. The Mylar targets were adjusted to reach temperatures that matched the apparent temperature of the background.

In the thermal image, the five targets are very difficult to identify. Most of the observers that were showed the images could identify only two of the five targets.

**Figure 10** shows the polarization image of the same targets take at the same instant. Of course all of the observers could identify all 5 targets. The polarization image is processed by painting pixels that show polarization above $s_1 > 0.02$ green. The unpolarized pixels remain grey level. The conditions for this test were clear sky with apparent sky temperature of approximately -30C. The ambient air temperature was approximately 25C. The sun azimuth with respect to the look angle was -90$^o$ and elevation angle was 20$^o$.

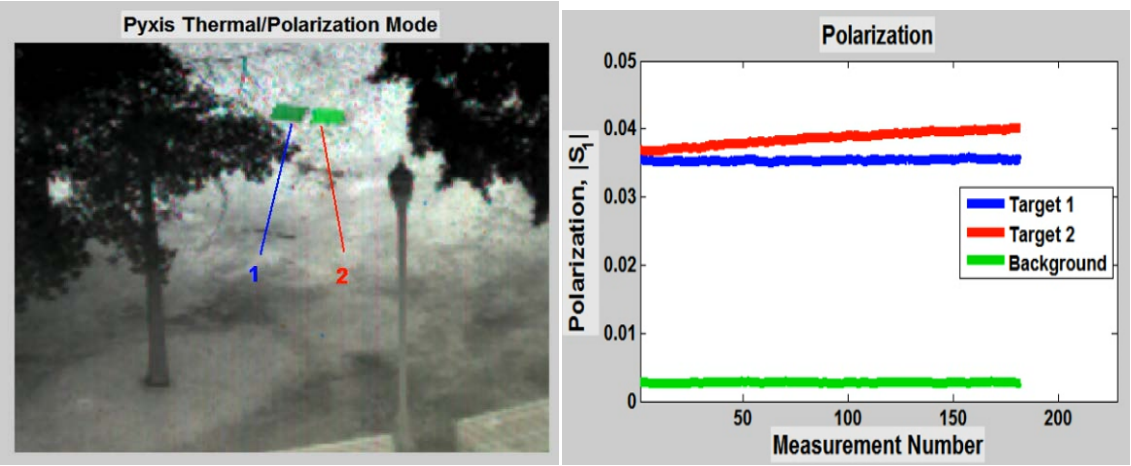


**Figure 8** s1 polarization image of targets during thermal cross-over point.


**Figure 9** Target set viewed in thermal mode


**Figure 10** Target set viewed in thermal/polarization mode

## 5. Discussion and Conclusion

Thermal imagers fall short when the apparent temperature of an object of interest matches its surroundings or in situations involving significant background clutter. These conditions occur in many applications involving acquisition and tracking of ground vehicles in high clutter, UAV, UAS detection against sky and earth backgrounds, detection of swimmers and vessels on water backgrounds, and many other thermal applications.

An imaging polarimeter provides both polarization sensing *and* thermal sensing. When environmental conditions result in poor thermal contrast, the polarization mode often provides additional contrast even when thermal contrast is zero. In addition, since the detection physics of the polarization mode is different than the thermal mode, objects are often more easily visualized in the polarization mode or hybrid polarization/thermal mode. For example, when attempting to acquire a man-made object against an earth background, the natural earth background is largely rejected polarization allowing the man-made object to standout in the image.

With recent advances in polarimetry and the availability small SWAP imaging polarimeters, integration onto platforms such as UAS's, ground vehicles and un-mounted soldiers is now possible. The application space of LWIR imaging polarimetry is expected to grow significantly in the coming years.

## References:


1. M. Felton, K. P. Gurton, J. L. Pezzaniti, D. B. Chenault, and L. E. Roth, "Measured comparison of the crossover periods for mid- and long-wave IR (MWIR and LWIR) polarimetric and conventional thermal imagery," Optics Express, Vol. 18, Issue 15, pp. 15704-15713 (2010).

2. C. An, J. Grantham, J. King, J. Robinson, L. Pezzaniti, K. Gurton, "Utility of Polarization Sensors for Clutter Rejection", 6th Annual US Missile Defense Conference, Washington DC, March 31-April 3, (2008).

3. K.P. Gurton, M. Felton, "Detection of buried Improvised Explosive Devices (IED) using passive long-wave infrared (LWIR) polarimetric imaging", ARL Technical Report, ARL-TR-4941 Sept. (2009).

4. J. S. Harchanko, D. B. Chenault, C. F. Farlow, and K. Spradley, "Detecting a surface swimmer using long wave infrared imaging polarimetry," in Photonics for Port and Harbor Security, M. J. DeWeert and T. T. Saito, eds., Proc. SPIE 5780 (2005).

5. M.W. Kudenov, E.L. Dereniak, J.L. Pezzaniti, "2-Cam LWIR imaging Stokes polarimeter," Polarization: Measurement, Analysis and Remote Sensing VIII, edited by D. B. Chenault, D. H. Goldstein, Proc. Of SPIE Vol. 6972, (2008).

6. B.M. Ratliff, D.A. Lemaster, R.T. Mack, P.V. Villenueve, J.J. Weinheimer,J.R. Middendorf, "Detection and tracking of RC model aircraft in LWIR microgrid polarimeter data, "*Proc. SPIE* 8160, Polarization Science and Remote Sensing V, 816002 (September 9, 2011)

7. www.polarissensor.com

8. S. Tyo, B.M. Ratliff, J. Boger, W. Black, D. Bowers, M. Fetrow, "The effects of thermal equilibrium and contrast in LWIR polarimetric images", Opt. Express, vol. 15, no. 23 Nov. (2007).

9. K.P. Gurton, M. Felton, "Detection of disturbed earth using passive LWIR polarimetric imaging" Proc SPIE Optics and Photonics Conference, San Diego, Ca. August 2-6, (2009).

10. O. Sandus, "A review of emission polarization," Appl. Opt. 4, 1634–1642 (1965).

11. K. P. Gurton, R. Dahmani, G. Videen, "Measured degree of infrared polarization for a variety of thermal emitting surfaces," Army Research Laboratory report , ARL-TR-3240, June 2004.